Lifetime of the $1s_2(^1P_1)$ and $1s_4(^3P_1)$ levels of neon by the cascade Hanle effect*

Natarajan D. Bhaskar†
Columbia University, New York, New York 10027

Allen Lurio
IBM Thomas J. Watson Research Center, Yorktown Heights, New York 10598

(Received 1 December 1975)

The theory of the cascade level-crossing effect as formulated by Happer is evaluated for zero-nuclear-spin atomic systems and extended to include the case of a polarized initial state. We have used this theory to interpret our cascade-Hanle-effect results (zero-field level crossings) to obtain the lifetime of the two resonance levels, $1s_2(^1P_1)$ and $1s_4(^3P_1)$, of the $2p^5 3s$ configuration of neon. The resonance lines 744 Å ($1s_4$-$^1S_0$) and 736 Å ($1s_2$-$^1S_0$) are produced in the cascade to the ground $^1S_0$ state when a beam of metastable $1s_3(^3P_0)$ and $1s_5(^3P_2)$ neon atoms is excited by selected lines of the $2p^5 3s$-$2p^5 3p$ transition array. Our results are $\tau(1s_2) = 1.65 \pm 0.16$ nsec and $\tau(1s_4) = 20.5 \pm 1.5$ nsec.

I. INTRODUCTION

The lifetimes of the $1s_4(^3P_1)$ and the $1s_2(^1P_1)$ resonance levels of neon have been the subject of considerable experimental[1-10] and theoretical investigation.[11-13] A variety of techniques were used in these measurements including Fabry-Perot determination of emission profile widths, exponential decay under pulsed-electron excitation or beam-foil excitation, and even lifetime lengthening due to imprisonment of resonance radiation. These measurements are all subject to interpretative complications[14-17]: radiative cascading in the case of impact excitation, collisional broadening in the case of emission profiles, and photon entrapment when the resonant photon passes through unexcited neon gas before being detected. A comparison of the various measurements of the lifetimes shows a wide discrepancy among the reported values. In view of these discrepancies we felt that the level-crossing technique, essentially free of the above-mentioned interpretative complications, could be fruitfully applied in the measurement of these lifetimes.

No cascade level-crossing studies involving the resonance levels of neon have been reported since the wavelengths of the lines from the $1s_4(^3P_1)$ and $1s_2(^1P_1)$ states to the ground state $^1S_0$ are 744 and 736 Å, respectively, and no structural transparent material exists at these wavelengths. Our experimental procedure was as follows: An atomic beam consisting of $1s_5(^3P_2)$ and $1s_3(^3P_0)$ metastable atoms of neon was produced by the electron bombardment of ground-state neon atoms. The metastable beam passed through a region of uniform variable magnetic field which was directed either along the beam or opposite to it. The $1s_5(^3P_2)$ and $1s_3(^3P_0)$ metastable atoms were selectively excited to one of the several $2p(2p^5 3p)$ states depending on the wavelength of the incident resonance radiation from the neon resonance lamp. The excited state will subsequently decay to one of the lower resonance levels $1s_4(^3P_1)$ or $1s_2(^1P_1)$ and also to the metastable state from which it was optically excited. The branching ratios for the decay to the various $2p^5 3s$ levels depends on the excited state; i.e., different excited states have different branching ratios. The fluorescent radiation of 744 Å ($1s_4$-$^1S_0$) and 736 Å ($1s_2$-$^1S_0$) resulting from the decay of the resonance levels to the ground state was detected as a function of the applied magnetic field. The magnetic width of this cascade Hanle signal depends sensitively on the lifetime and g value of the excited state and the resonance levels.

The low-lying levels of neon spectra are shown in Fig. 1 and those levels and lines involved in the present experiment are shown in Fig. 2. Throughout this paper the levels of neon will be designated by Paschen notation. The LS designation of states shown within the brackets is only for convenience in identifying the states.

II. THEORY

Cascade-Hanle-effect signal. The theory of cascade-Hanle-effect experiments is similar to the theory of level-crossing spectroscopy and has been treated in the pioneering work in this technique by Gupta, Chang, and Happer.[18] We shall use their notation in this paper.

Four atomic states are involved in the experiment (see Fig. 3), and we shall call these states i (initial), e (excited), b (branch), and f (final). In the present experiment the nuclear spin I is zero. We shall designate the electronic angular momenta in the initial, excited, branch, and final states by J_i, J_e, J_b, and J_f, respectively. Initial-

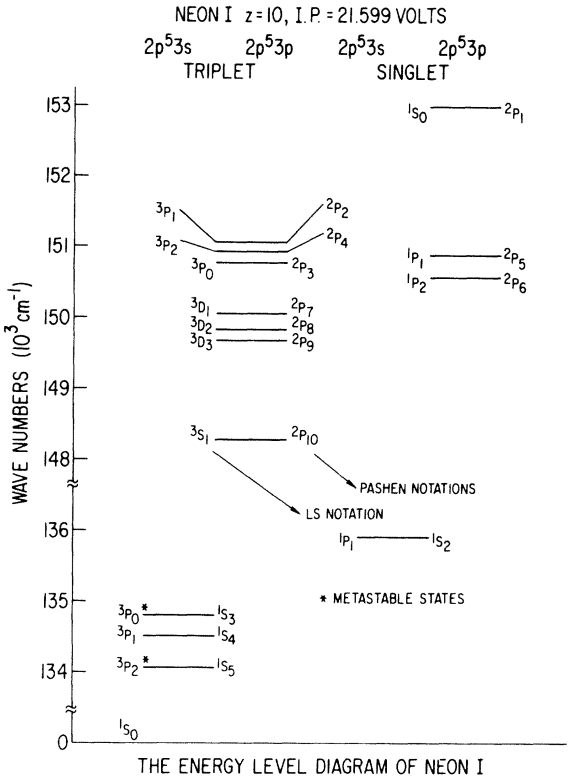

FIG. 1. Energy-level diagram of neon showing 2s and 2p levels.

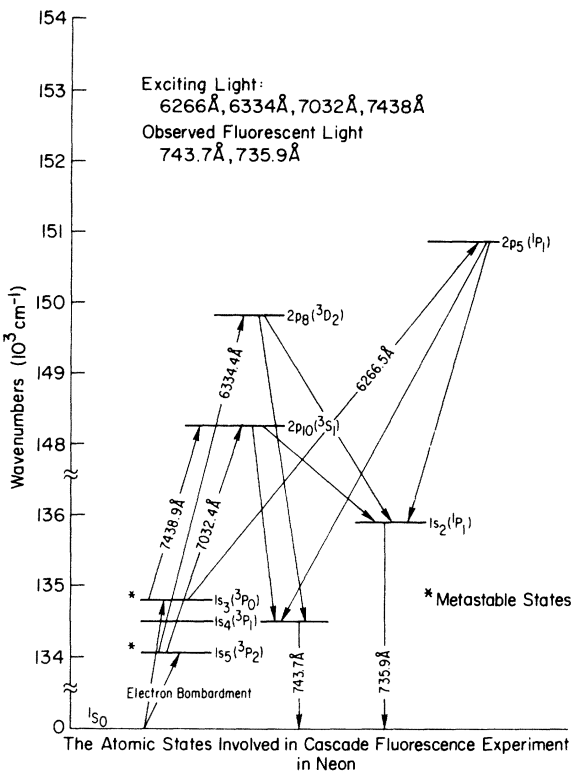

FIG. 2. Atomic states and lines involved in our cascade level-crossing experiment.

state atoms are transferred into the excited state by a beam of polarized resonance radiation. Excited-state atoms decay spontaneously into the branch state, but we do not observe the visible fluorescent radiation which is produced by the decay $e \rightarrow b$. The branch-state atoms decay spontaneously to the final state, and we do observe the unpolarized fluorescent light (XUV radiation) which is produced by the decay $b \rightarrow f$. This cascade fluorescent-light intensity depends on the properties of the four atomic states.

A. Theory for unpolarized ground state

In our treatment we shall adopt a density-matrix approach to evaluate the cascade Hanle effect. The present theoretical discussion is a slightly revised version of the theory given to the authors by Happer.[19] While we have made use of some formulas given by Gupta, Chang, and Happer in their work on the alkali metals, two differences between our experiment and theirs necessitate a modification of their theory. These are as follows: (1) Neon has a zero nuclear spin so a complete reduction of all angular integrals can be made; and (2) because we produce our initial state by electron bombardment, the possibility exists that the ground state is aligned so that one must consider the consequences of alignment on the Hanle signal.

The starting point for the calculation of the cascade Hanle effect when alignment or coherence exists in the ground state is the density-matrix equation

$$\frac{d\rho}{dt} = -\Gamma\rho + \frac{1}{i\hbar}[\mathcal{H}_0, \rho] + \frac{d^{(2)}\rho}{dt}. \tag{1}$$

In this equation the first term $d\rho/dt$ is the total rate of change of the density matrix, $-\Gamma\rho$ is the rate of decay due to spontaneous emission, $(1/i\hbar)[\mathcal{H}_0, \rho]$ is the rate of change of phase due to evolution under the zero-order Hamiltonian, $\mathcal{H}_{\text{hfs}} + \mathcal{H}_{\text{Zeeman}}$, and $d^{(2)}\rho/dt$ is the rate of increase of population by optical excitation *to* the state, or spontaneous decay *into* the state.[19] The levels involved in our derivation are shown in Fig. 3. This equation for the excited state becomes

$$\frac{d\rho^e_{mn}}{dt} = -\Gamma_e \rho^e_{mn} - i\omega^e_{mn}\rho^e_{mn} + \sum_{\mu,\nu}\left(\frac{2\pi\tilde{U}e^2}{m^2\omega^2_{ie}\hbar^2}\right)\hat{e}\cdot\vec{P}_{m\mu}\rho^i_{\mu\nu}\vec{P}_{\nu n}\cdot\hat{e}^*, \tag{2}$$

and for the branch state becomes

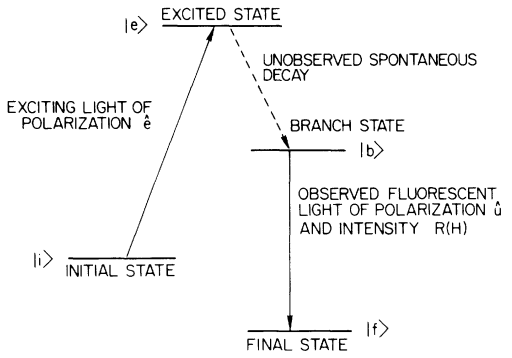

FIG. 3. Diagram of levels i, e, b, f, involved in theoretical expression.

$$\frac{d\rho^b_{\alpha\beta}}{dt} = -\Gamma_b \rho^b_{\alpha\beta} - i\omega^b_{\alpha\beta}\rho^b_{\alpha\beta} + \left(\frac{4e^2\omega_{eb}}{3m^2c^3\hbar}\right)\sum_{m,n}\vec{P}_{\alpha m}\rho^e_{mn}\vec{P}_{n\beta}, \tag{3}$$

where we use the notation $\vec{P}_{m\mu} = \langle m|\vec{P}|\mu\rangle$ and $\omega^e_{mn} = (E^e_m - E^e_n)/\hbar$. The last term in Eq. (2) may be obtained by forming the density-matrix equation from Eqs. (II.9), (II.31), (II.32), and (II.33) in the paper by Happer and Mathur[20] and taking the limit as t becomes large so that $e^{-\Gamma t/2} \to 0$. We have also assumed that the exciting spectral profile be uniform.

The rate of emission of photons into solid angle $d\Omega$ which arises from the decay of the branch state may be derived from Fermi's "golden rule," and is

$$R\,d\Omega = \frac{e^2\omega_{bf}}{2\pi m^2c^3\hbar}\sum_{i,\alpha,\beta}\hat{u}^*\cdot\vec{P}_{i\alpha}\rho^b_{\alpha\beta}\vec{P}_{\beta i}\cdot\hat{u}\,d\Omega\,. \tag{4}$$

If Eq. (4) with b and f replaced by e and b, respectively, is integrated over all angles and polarizations, one obtains the last term in Eq. (3), which is appropriate since we do not observe any excited to branch-state photons. Under steady-state conditions $d\rho^e_{mn}/dt = d\rho^b_{\alpha\beta}/dt = 0$; so Eqs. (2) and (3) may be solved and substituted into Eq. (4) yielding

$$R = \frac{4e^6\omega_{eb}\omega_{bf}}{3m^6c^6\hbar^4\omega^2_{ie}}\tilde{U}\sum_{\substack{\alpha,\beta\\ m,n\\ \mu,\nu,i}}\frac{(\hat{u}^*\cdot\vec{P}_{i\alpha})\vec{P}_{\alpha m}\cdot(\hat{e}\cdot\vec{P}_{m\mu}\rho^i_{\mu\nu}\vec{P}_{\nu n}\cdot\hat{e}^*)\vec{P}_{n\beta}(\vec{P}_{\beta i}\cdot\hat{u})}{(\Gamma_e + i\omega^e_{mn})(\Gamma_b + i\omega^b_{\alpha\beta})}\,. \tag{5}$$

This result simplifies for the case of the unpolarized ground state as

$$\rho^i = \frac{1}{2J_i+1}\sum_\mu |J_i\,\mu\rangle\langle J_i\,\mu|\,,$$

so that

$$\hat{e}\cdot\vec{P}|\mu\rangle\rho^i_{\mu\nu}\langle\nu|\hat{e}^*\cdot\vec{P} = \frac{1}{2J_i+1}\hat{e}\cdot\vec{P}|\mu\rangle\langle\mu|\hat{e}^*\cdot\vec{P}\,. \tag{6}$$

We may now evaluate the middle and outer pairs of matrix elements in Eq. (5) by using the expression

$$\sum_\mu \hat{e}\cdot\vec{P}|\mu\rangle\langle\mu|\hat{e}^*\cdot\vec{P} = \frac{3m\omega_{ie}\hbar f_{ie}}{2}(2J_i+1)\sum_{L,M}(-1)^{L+M}W(J_iJ_e1L;1J_e)E^L_{-M}(\hat{e},\hat{e}^*)T^L_M(J_eJ_e)\,, \tag{7}$$

where we have made use of

$$f_{ie} = \Gamma_{ei}\frac{mc^3}{2e^2\omega^2_{ie}}\frac{2J_e+1}{2J_i+1} = \frac{2m\omega_{ie}}{3\hbar e^2}\left(\frac{2J_e+1}{2J_i+1}\right)^{1/2}(-1)^{J_e-J_i}\langle J_e\|P\|J_i\rangle\langle J_i\|P\|J_e\rangle_{\text{Rose}}\,. \tag{8}$$

Here, f_{ie} is the absorption oscillator strength from state i to state e and Γ_{ei} is the partial decay rate from state e to state i.

The subscript "Rose" in Eq. (8) means that the reduced-matrix element is that defined by Rose[21] rather than that defined by Racah. Another necessary relation for simplifying Eq. (5) is

$$\vec{P}\cdot T^L_M(J_eJ_e)\vec{P} = \frac{3m^2c^3\hbar\,\Gamma_{eb}(2J_e+1)}{4e^2\omega_{eb}} \times T^L_M(J_bJ_b)W(1J_eJ_bL;J_bJ_e)\,, \tag{9}$$

where W is the Racah coefficient and T^L_M is defined by Happer.[18] When we use Eqs. (6)–(9) to evaluate Eq. (5), we obtain the satisfying result

$$R = \sum_{L,M}(-1)^M\frac{B_LE^L_MU^L_{-M}}{(\Gamma_e + iM\omega^e)(\Gamma_b + iM\omega^b)}\,, \tag{10}$$

where

$$B_L = (9R_0/8\pi)\Gamma_{eb}\,\Gamma_{bf}(2J_e+1)(2J_b+1) \times W(J_iJ_e1L;1J_e) \times W(1J_eJ_bL;J_bJ_e)W(1LJ_fJ_b;1J_b)\,, \tag{11}$$

$$R_0 = \pi e^2 f_{ie} \bar{U}/m\omega_{ie}\hbar\,,$$
$$E^L_M = \sum_m e_m (e_{m-M})^* (-1)^{m-M-1} C(11L; m, M-m)\,. \tag{12}$$

U^L_M, the polarization tensor of the detected light, is defined by an equation similar to that for E^L_M.

B. Case of polarized ground state

Equation (5) is still valid for the general case where polarization exists in the ground state. We must now, however, resolve the ground-state density matrix into spherical tensor components via the relation

$$\rho^i = \sum_{LM} (-1)^M \rho^L_M (J_i J_i) T^L_{-M}(J_i J_i)\,.$$

The following three relations enable us to simplify the middle-bracketed term in Eq. (5):

$$\vec{P}\cdot T^L_M(J_i J_i)\vec{P} = \sum_{L'\Lambda} (-1)^{J_e - J_i}[(2J_i+1)(2\Lambda+1)(2L'+1)]^{1/2} \langle J_i \| P \| J_e\rangle\langle J_e \| P \| J_i\rangle_{\text{Rose}} \times \begin{bmatrix} 1 & J_e & J_i \\ 1 & J_e & J_i \\ L' & \Lambda & L \end{bmatrix} [Q^{L'} T^\Lambda(J_e J_e)]_{LM}\,, \tag{13}$$

$$\hat{e}\cdot[Q^{L'} T^\Lambda]_{LM} \hat{e}^* = [E^{L'} T^\Lambda]_{LM}\,, \tag{14}$$

$$(\hat{e}\cdot\vec{P})\rho^i(\vec{P}\cdot\hat{e}^*) = \tfrac{3}{2} m\hbar\omega_{ie} f_{ie}(2J_i+1) \sum_{L,L',\Lambda} (-1)^{L'}[(2L+1)(2L'+1)]^{1/2} \begin{bmatrix} 1 & J_e & J_i \\ 1 & J_e & J_i \\ L' & \Lambda & L \end{bmatrix} T^\Lambda\cdot[E^{L'}(\rho^i)^L]_\Lambda\,, \tag{15}$$

where Q_L is defined by Happer and Mathur[20] in their Appendix. Comparing Eqs. (6), (7), and (15), we see that if we replace E^L_{-M} in Eq. (7) by $\mathcal{E}^L_{-M}$ where $\mathcal{E}^L_M$ is defined by the expression

$$\mathcal{E}^L_M = (2J_i+1) \sum_{\Lambda L'} (-1)^{L'-L} \frac{[(2\Lambda+1)(2L'+1)]^{1/2}}{W(J_i J_e 1L; 1J_e)} \begin{bmatrix} 1 & J_e & J_i \\ 1 & J_e & J_i \\ L' & L & \Lambda \end{bmatrix} [E^{L'}(\rho^i)^\Lambda]_{LM}\,, \tag{16}$$

then the rest of the analysis proceeds as in Sec. II A resulting again in Eq. (10) but with $\mathcal{E}^L_M$ replacing E^L_M. If we expand Eq. (16) by separating out the $\Lambda = 0$ term, we obtain

$$\mathcal{E}^L_M = E^L_M + \sum_{\Lambda=1}^{2J_i} \sum_{L'=0}^{2} (-1)^{L'-L} \frac{(2J_i+1)[(2\Lambda+1)(2L'+1)]^{1/2}}{W(J_i J_e 1L; 1J_e)} \begin{bmatrix} 1 & J_e & J_i \\ 1 & J_e & J_i \\ L' & L & \Lambda \end{bmatrix} [E^{L'}(\rho^i)^\Lambda]_{LM}\,, \tag{17}$$

which shows that $\mathcal{E}^L_M$ reduces to E^L_M for an unpolarized ground state since $(\rho^i)^0 = 1/(2J_i+1)^{1/2}$ and all other $(\rho^i)^L = 0$.

In Appendix B we discuss further the effect of alignment on the Hanle signal.

III. EXPERIMENT

A. Apparatus

The atomic-beam apparatus used in this experiment has been described in detail by Burger and Lurio.[22] A beam of metastable neon atoms is produced by electron bombardment of the ground-state neon atoms in the source chamber of the atomic-beam apparatus. The energy of the bombarding electrons is much greater than the threshold for the metastable production and therefore atoms in the higher excited states are also produced. These excited states, being very short lived, decay directly or by cascade to the metastable and ground-state emitting photons. The beam we observe, therefore, consists of metastable- and ground-state atoms traveling with a mean velocity of 6.6×10^4 cm/sec. In the interaction chamber the atoms in one of the metastable states are optically excited by linearly polarized resonance light of appropriate frequency. A static magnetic field is maintained along the direction of the beam by a pair of Helmholtz coils. The component of the stray magnetic fields in the

plane perpendicular to the beam is cancelled to almost zero by two pairs of compensating Helmholtz coils.

The neon resonance lamp, a quartz cell of 22 mm outer diameter and 10 mm path length, is mounted at the end of a tunable Evenson cavity driven by a 2450-MHz microwave power source. The microwave power is empirically adjusted and the cavity tuned to obtain maximum intensity in the resonance lines of interest. The optimum intensity of the various lines for various different conditions of the resonance lamp and microwave power was measured in a separate experiment using a grating spectrometer and a photomultiplier tube. The neon in the resonance cell was filled to a pressure of 10 mm of Hg. The light from the resonance cell was focussed into the interaction region using a simple f-1 optical arrangement of two condensing lenses, and was linearly polarized using a commercial polaroid: type HN32. The visible spectrum of neon consists of many closely spaced lines. The resonance lines of interest (6266, 6334, 7032, and 7438 Å) are isolated using narrow-band interference filters. Our selection of these lines is just due to the fact that these are the only lines that can be reasonably well isolated with interference filters. The interference filters are mounted just outside the quartz window in the interaction chamber rather than just in front of the resonance lamp because the transmission curve of the interference filter gets broadened with the angular spread of the incident cone of light. The effectiveness of the interference filter in blocking the neighboring closely spaced lines from the line of interest was also tested using a monochromator. A Schott RG715 (10 mm thick) colored-glass filter was also used for the 7438-Å line.

The magnetic field at the center of the interaction region was measured by a transverse Hall probe and the component of the stray magnetic field in the plane perpendicular to the beam direction was cancelled to less than 5 mG. A small correction to the main field due to nonzero component of the stray field along the beam direction was also applied. Since magnetic fields of no more than 13 G were ever applied, no water cooling was needed, and the main magnet assembly was conveniently located inside the vacuum chamber. Over the volume of interest in the interaction region, the magnetic field was homogeneous to better than 2%.

A channeltron electron multiplier which is insensitive to the visible photons (incident resonance radiation) is used to detect the cascade-fluorescent XUV photons (744 and 736 Å). The channeltron is located 8–10 cm from the center of the interaction region perpendicularly above the beam. Since the magnetic fields employed are no greater than 13 G, no magnetic shielding of the channeltron is required and the gain of the electron multiplier unaffected. This was tested in two ways. As shown in Appendix A, the cascade fluorescent signal has no magnetic field dependence when the incident resonance light is polarized parallel to the magnetic field, and any dependence of channeltron detected signal on the magnetic field would arise entirely due to the dependence of the gain of the channeltron on the magnetic field. It was observed that the detected signal averaged over many sweeps of the magnetic field showed no detectable dependence on the field. The channeltron was irradiated by the 2537-Å Hg line to which it is sensitive, and the channeltron signal averaged over several thousand sweeps of the magnetic field also showed no field dependence. The channeltron is shielded from ions by a stack of thin parallel copper plates (3.2 mm apart and 2.5 cm deep) which were alternately biased at 0 and +100 V. To minimize the background signal, the channeltron is out of the direct line with any wide-angle portion of the beam.

The metastable beam was monitored by measuring with a picoammeter, the current of ejected electrons which resulted when the metastable atoms impinged on a gold target. The details regarding the electron-bombarder gas-handling sys-

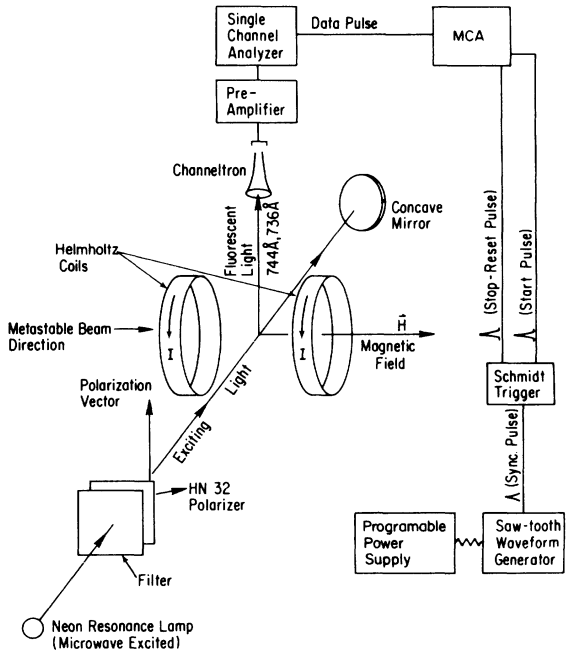

FIG. 4. Details of experimental arrangement and measurement technique.

tem and other pertinent specifications of the apparatus have been described previously.[22]

B. Technique of measurement

The technique of measurement is indicated in the block-diagram form in Fig. 4. A saw-tooth wave is used to drive a Kepco BOP36-5M programmable power supply which provided the current for the main pair of Helmholtz coils. Since no unilateral drift either in the beam or in the incident resonance light was detected during the course of a run, a saw-tooth wave instead of a symmetrical triangular wave was used to sweep the magnetic field. A trigger pulse generated at the beginning of each sweep was used to generate the control commands for the multichannel analyzer (MCA) used for data accumulation. Drifts in metastable beam and lamp intensity were small and averaged out over a large number of sweeps. Typically, a run consisted of 5000 sweeps of the magnetic field lasting for approximately 12 h of data accumulation. This enabled us to measure small field-dependent effects in the signal such as the difference between the asymptotic value and the minimum value of the cascade fluorescent signal. The random variations being averaged out, the statistical noise in the accumulated counts was usually less than half a percent. The magnet power supply, the sweep generator, etc., were found to have no detectable instability or drift during the course of a run.

The magnetic field produced by the Helmholtz coils was determined from the voltage drop across a precision 1-Ω resistor in series with the coils. To determine the varying magnetic field, the output across the 1-Ω standard resistor was fed into the MCA in the "analog" mode for five sweeps of the field. The magnetic field was measured before and after each run, and no noticeable drifts were present.

The Bell 640 gaussmeter in combination with the temperature compensated probe has a quoted accuracy on the 0–30 G range of 0.05% of the full scale value plus 0.5% of the reading. The estimated accuracy of the magnetic field measurement is about a percent. The error in field measurement introduced by the use of the MCA was small, as was verified by measuring known static fields.

C. Measurements and results

The experimental data consisted of the intensity of the cascade-fluorescent photons (744 and 736 Å) and background due to the metastable beam as a function of the applied magnetic field, for the incident resonance light linearly polarized perpendicular to the magnetic field. The beam background in the absence of the exciting light did not show any detectable dependence on the magnetic field. The conditions in the electron bombarder were found to affect the beam background, but no quantitative conclusions could be drawn. Since the channeltron is shielded from the charged particles, the beam background was concluded to be due to the photons originating in the electron-bombarder region and also to the collisional deexcitation of the metastable atoms with the residual gas atoms. The pressure in the interaction chamber was typically 5×10^{-8} Torr. A detailed investigation of this beam background was undertaken by Burger and Lurio[22] in their lifetime measurements in helium, and we believe their conclusions are equally applicable in our present work. Typical beam-background counting rate for a metastable beam of 8×10^8 atoms/sec is about 10/sec, much greater than the dark current of the channeltron which is about 0.1/sec. For all the incident resonance lines studied except the 7438-Å line, the cascade-fluorescent photon counting rate was at least 15 times greater than metastable beam background. For the 7438-Å line the ratio of the fluorescent-light signal to beam background was at best 2:1. In light of this and the small field dependence of the signal, long integration times were required. The scatter of the experimental data was very small and within the expected statistical fluctuations.

As shown in Appendix A, the theoretical cascade-fluorescence signal as a function of the applied magnetic field for the decay of an excited state e through two branch states b and b' is given by

$$R(H)=A+B\left(\frac{1-4(\mu_0H/\hbar)^2g_e\tau_e g_b\tau_b}{[1+4(g_e\tau_e\mu_0H/\hbar)^2][1+4(g_b\tau_b\mu_0H/\hbar)^2]}+\frac{\gamma[1-4(\mu_0H/\hbar)^2g_e\tau_e g_{b'}\tau_{b'}]}{[1+4(g_e\tau_e\mu_0H/\hbar)^2][1+4(g_{b'}\tau_{b'}\mu_0H/\hbar)^2]}\right). \quad (18)$$

Here, A and B are constants which account for the light-independent background and for the arbitrary amplitude of the light-induced signal. For neon, b and b' correspond to the $1s_2$ and $1s_4$ states. In Table I are listed the partial decay rates Γ_{eb} from which the branching factor $\gamma=\Gamma_{eb'}/\Gamma_{eb}$ can be evaluated. As can be seen from our table, each excited state decays predominantly to only one branch state; the γ factors to the less-populated branch state being $\gamma(2p_5)=0.031$, $\gamma(2p_8)=0.096$, and $\gamma(2p_{10})=0.012$. Thus to an excellent approximation we can consider only the decay of the ex-

TABLE I. Partial decay rates and branching factors. Results are from Ref. 23.

Initial state	Branch state	Partial decay rate (10^7 sec^{-1})	Branching factor γ
$2p_5$	$1s_2$	2.17	
$2p_5$	$1s_4$	0.067	0.029
$2p_8$	$1s_2$	0.287	0.096
$2p_8$	$1s_4$	3.00	
$2p_{10}$	$1s_2$	0.012	0.012
$2p_{10}$	$1s_4$	0.935	

cited state through the dominant branch state. This is essential as otherwise we will have too many parameters to determine meaningfully from the experimental signal-to-noise ratio of our data. After finding the best-fit parameters for the single decay-mode approximation, we can correct for the small effect of branching on our results.

We could now fit our data by the theoretical expression given in Eq. (18) with the γ term omitted. When, however, we examine the form of Eq. (18) with the γ term omitted, we see that it is completely symmetric in $g_e\tau_e$ and $g_b\tau_b$ depending only on the product and sum square of these quantities. Hence, the result of least-squares fitting our experimental data to this theoretical function will be two sets of values for $g_e\tau_e$ and $g_b\tau_b$, i.e., $g_e\tau_e=\alpha$, $g_b\tau_b=\beta$ and $g_e\tau_e=\beta$, $g_b\tau_b=\alpha$. To decide between these solutions is not possible unless one has some prior information on the relative size of the lifetimes.

Since the lifetimes of the $2p$ states have been measured by a number of different people and with excellent agreement between their results, we decided to fix $g_e\tau_e$ in our fitting procedure and solve for $g_b\tau_b$. The values we adopted are given in Table II. For the 7032- and 7438-Å lines very consistent results were obtained, which yielded a value of $\tau(1s_4)=20.5\pm1.5$ nsec. Typical data and fits to

TABLE II. Lifetimes and g_J factors of $2p$ states involved in present experiment. Results are averaged values from Ref. 23.

Exciting-light wavelength (Å)	Excited state	Excited-state lifetime (nsec)	g_J value of excited state
6217	$2p_7$	19.8	0.669
6266	$2p_5$	19.7	0.999
6334	$2p_8$	20.0	1.137
7032	$2p_{10}$	26.6	1.984
7438	$2p_{10}$	26.6	1.984

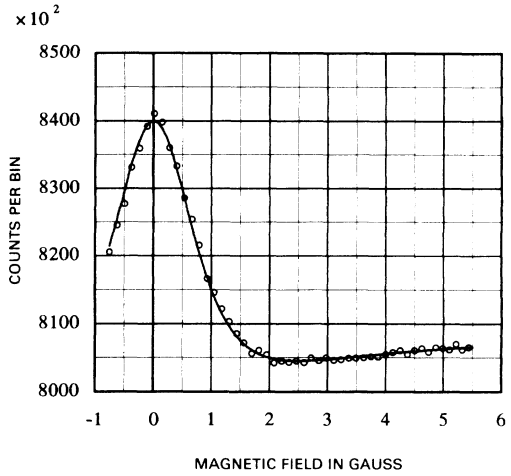

FIG. 5. Typical data and theoretical fit to 7032-Å line.

the data are shown in Figs. 5 and 6. Branching did not introduce any change in this result. Our uncertainty was estimated in two ways: first from a histogram of the τ values obtained from a fit to 33 runs on the 7438-Å line and 10 runs on the 7032-Å line, and second from a plot of χ^2 vs $g_b\tau_b$ in which the remaining parameters were optimized at each step. This procedure is discussed by Bevington[24] and Arndt and MacGregor.[25]

A similar approach on the 6266- and the 6334-Å line gave poor fits to the data with regions of data lying off the theoretical curve. This is illustrated in Fig. 7 for the 6266-Å line. A careful study of our experimental procedure was undertaken. Our first thought was that alignment might be produced in the electron gun which would distort the Hanle signal. This was the motivation for our derivation

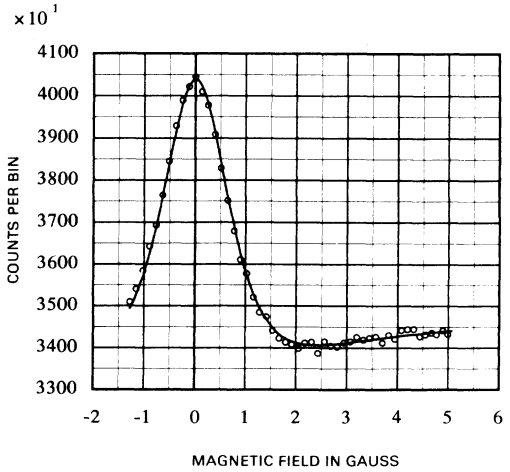

FIG. 6. Typical data and theoretical fit to 7438-Å line.

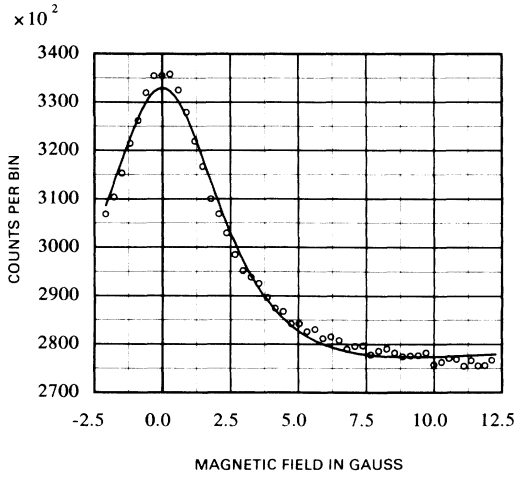

FIG. 7. Typical data and theoretical fit to 6266-Å line.

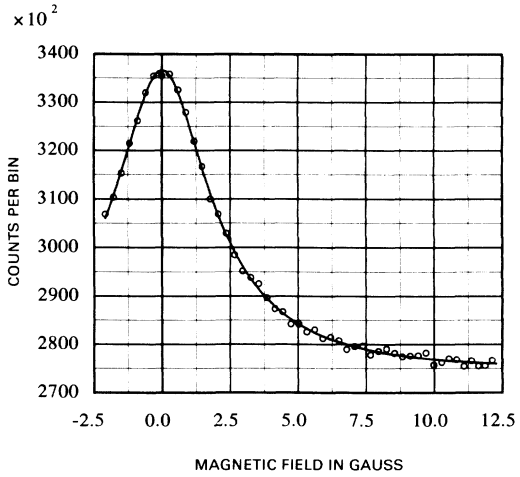

FIG. 8. Typical data and theoretical fit to 6266-Å line including leakage of 6217-Å line through interference filter.

of the Hanle signal when alignment is present in the initial state. This analysis shows (see Appendix B) that alignment will not distort the Hanle line shape. As we shall show convincingly in what follows, the problem actually arises from incomplete isolation of the exciting line from the lamp. There are three strong neon resonance lines in the region of interest which can excite the metastable neon beam, namely, 6217, 6266, and 6334 Å. The transmission band of an interference filter broadens and shifts to shorter wavelengths for light not normally incident on the filter. Our focusing arrangement used for f-1 optics with the consequence that some 6217 Å light is transmitted along with the 6266-Å line and some 6266-Å light along with the 6334-Å line, each pair of lines branch predominantly to different states. Let us consider the 6266-Å exciting line first. The Hanle effect of the 6217-Å interfering line is completely known from results in Table II and our value $\tau(1s_4) = 20.5$ nsec. (The filters completely isolate

TABLE III. Summary of all lifetime measurements of the $1s_2$ and $1s_4$ levels of neon.

$\tau(1s_2)$ (nsec)	$\tau(1s_4)$ (nsec)	Year	Author (Ref.)	Experimental technique
	16± 8	1933	N. Schutz (1)	Natural linewidth
	20	1955	V. Phelps (2)	Imprisonment of resonance radiation
1.51± 0.14	20.8± 3.5	1967	H. Kuhn, E. Lewis, and E. Lewis (4)	Corrected self-broadening of resonance radiation
1.87± 0.18	31.7± 1.6	1969	G. Lawrence and H. Liszt (5)	Decay after pulsed electron excitation
1.81± 0.14		1970	J. De Jongh and J. Van Eck (6)	Self-absorption
	18± 1	1971	S. Kazantsev and M. Chaika (7)	Alignment in a discharge tube
1.3 ± 0.1	29.8± 2	1971	J. Kernahan, A. Denis, and R. Drouin (8)	Beam foil
1.54± 0.06		1973	D. Irwin, A. Livingston, J. Kernahan (9)	Beam foil
1.51± 0.1	31.2± 3	1974	E. Knystautas and R. Drouin (10)	Beam foil
1.65± 0.16	20.5± 1.5	1975	N. Bhaskar and A. Lurio	Cascade level crossing

TABLE IV. Calculated values for the lifetime (in nsec) of the $1s_2$ and $1s_4$ levels of neon.

$\tau(1s_4)$	$\tau(1s_2)$	Author (Ref.)
20–27	2.07–2.74	A. Gold and R. Knox (11)
20–24.5	1.26–1.8	P. Gruzdev and A. Loginov (13)
20.3–24.4	1.56–1.91	M. Aymar, S. Feneuille, and M. Klapisch (12)

the 7032- and 7438-Å lines.) Only the amount of signal leaking through the 6266-Å filter is unknown. With this amplitude as a free parameter we refitted our data and found that the least-squares residual dropped by a factor of 7, an excellent fit to the data resulted, and the fit was quite sensitive to the mixing amplitude and the lifetime of the $1s_2$ state. In Fig. 8 we show the same data as in Fig. 7 but with 32% admixture of 6217-Å light. All 6266-Å line runs were reanalyzed with the result $\tau(1s_2) = 1.65 \pm 0.16$ nsec. A reanalysis of the 6334-Å line data also gave excellent fits and results consistent with 20.5 nsec for the $1s_4$ state.

IV. DISCUSSION OF RESULTS

A summary of all known measurements of the lifetime of the $1s_4$ and $1s_2$ levels of neon is given in Table III. We may make several observations on these results. The first two measurements are historical and should not be considered in the same light as the more recent results. The results for the $1s_4$ state divide into two groups with values near 20 nsec and values near 30 nsec. All the values near 30 arise from decay measurements in which a number of excited states are initially populated many of which cascade through the $1s_4$ state. It appears that the time-dependent filling of the $1s_4$ state is not properly accounted for in these measurements leading to their excessive lifetime values. Results for the $1s_2$ state interestingly do not show this trend.

For comparison, the theoretical predictions for the lifetimes are given in Table IV.

Of all the techniques used to measure neon lifetimes, the level-crossing method described in this paper is most free of corrections provided isolated resonance lines are used in excitation. Such lines are easily obtained with a dye laser (one was not available to us) as shown by Dunning, Cook, West, and Stebbings.[26] We anticipate that the resonance lines of all the noble gases will shortly be measured with better than 2% precision in the near future using dye lasers and level-crossing techniques.

ACKNOWLEDGMENTS

The authors wish to thank Professor W. Happer for a number of illuminating discussions on the theory of cascade level crossings. We also would like to thank Dr. A. Khadjavi for his collaboration during the preliminary stages of the experiment.

APPENDIX A

We will derive here the expression for the observed cascade Hanle signal as a function of the external magnetic field H, the polarization of the exciting light, and the lifetimes of the excited state (τ_e) and branch state (τ_b) for the various initial states involved in the present experiment. The intensity of the cascade fluorescent photons is given in Eq. (10). The coefficient B_L which occurs in the cascade fluorescence signal R in Eq. (10) is independent of the external field; it only determines the sign and the magnitude of the signal. The magnetic-field dependence of the cascade fluorescence signal comes about through the two resonance denominators in which ω_b and ω_e are the Lamor frequencies of the branch and excited states, respectively:

$$\omega_b = Hg_b(e/2mc) \tag{A1}$$

and similarly for ω_e. The predicted signal agrees with our intuitive idea of the process when, for example, one of the levels has a very short lifetime. Consider the case when $\Gamma_b \gg \Gamma_e$ so that the second factor in the denominator of Eq. (10) hardly varies as ω_e ranges from 0 to Γ_e. Under that condition

$$R = \sum_{LM} (-1)^M B_L \frac{E_M^L U_{-M}^L}{(\Gamma_e + i\omega_e M)\Gamma_b}, \quad \Gamma_b \gg \Gamma_e, \tag{A2}$$

which is almost the same as the pure Hanle effect of the excited state. This can be understood as follows: Consider a magnetic field such that $\Gamma_e \ll \omega_e M$ and $\Gamma_b \gg \omega_b M$. Then in the presence of this field the initially excited linear combination of states will undergo a large change of phase while in state e, whereas it will undergo only a negligible change of phase in the state b. Thus the observed photon will carry information principally about the lifetime and g_j values of state e. Similarly in the other extreme case $\Gamma_e \gg \Gamma_b$:

$$R = \sum_{LM} (-1)^M B_L \frac{E_M^L U_{-M}^L}{(\Gamma_b + i\omega_b M)\Gamma_e}, \tag{A3}$$

i.e., almost the same as a pure Hanle effect in the branch state.

The atomic states involved in our present cascade fluorescence experiment in neon is shown in Fig. 2 along with the wavelength of the exciting light and the detected fluorescent light.

We shall evaluate Eq. (10) for various cases of the initial, excited, and branch states. In the neon spectra the actual coupling is much closer to the

TABLE V. $J_i=2$, $J_e=1$, $J_b=1$, $J_f=0$.

L	$W(211L;11)$	$W(111L;11)$	$W(L110;11)$	$B_L/\Gamma_{eb}\Gamma_{bf}R_0$
2	$\frac{1}{30}$	$-\frac{1}{6}$	$\frac{1}{3}$	$-3/160\pi$
1	$-\frac{1}{6}$	$\frac{1}{6}$	$\frac{1}{3}$	$-3/32\pi$
0	$\frac{1}{3}$	$\frac{1}{3}$	$\frac{1}{3}$	$3/8\pi$

TABLE VII. $J_i=0$, $J_e=1$, $J_b=1$, $J_f=0$.

L	$W(011L;11)$	$W(111L;11)$	$W(L110;11)$	$B_L/\Gamma_{eb}\Gamma_{bf}R_0$
2	$\frac{1}{3}$	$-\frac{1}{6}$	$\frac{1}{3}$	$-3/16\pi$
1	$\frac{1}{3}$	$\frac{1}{6}$	$\frac{1}{3}$	$3/16\pi$
0	$\frac{1}{3}$	$\frac{1}{3}$	$\frac{1}{3}$	$3/8\pi$

j-j scheme than to the L-S coupling scheme. For electric dipole transitions the following selection rules apply: change of parity, $\Delta J=0\pm1$, $\Delta M_J=0,\pm1$, and $J=0\rightarrow J=0$ forbidden. In our present experiment the electronic angular momentum of the various states are for the initial state $J_i=0$ or 2, for the excited state $J_e=1$ or 2 (transitions to states $J_e=3$ are possible but do not lead to a cascade), for the branch state $J_b=1$, and for the final state $J_f=0$. The values of the various Racah coefficients used in evaluating the coefficient B_L given in Eq. (10) for $L=2$, 1, 0 are listed in Tables V–VII.

The components of the exciting and detected fluorescent light polarization tensors E_M^L and U_M^L, respectively, can be expressed as

$$E_M^L=\sum_{m=0,\pm1} e_m e^*_{m-M}(-1)^{m-M-1}C(11L;m,M-m), \tag{A4}$$

where $\hat{e}$ is the complex polarization vector of the exciting light. In terms of Cartesian axes, the magnetic field is along the y axis, the direction and polarization of the exciting light is along the x and z axes respectively, and the direction of the detected unpolarized cascade-fluorescent light is along the z axis. The components of the exciting-light polarization tensor for the case in which the exciting light is polarized *perpendicular* to the magnetic field are

$$\begin{aligned} &E_2^2=E_{-2}^2=\tfrac{1}{2}, \quad E_1^2=E_{-1}^2=0, \quad E_0^2=1/\sqrt{6}, \\ &E_1^1=E_{-1}^1=E_0^1=0, \quad E_0^0=1/\sqrt{3}. \end{aligned} \tag{A5}$$

The detection of unpolarized fluorescent light is obtained by summing the contribution due to the two mutually orthogonal polarizations of the fluorescent light. The components of the fluorescent light polarization tensor U_M^L for the case in which the detected light is polarized normal to the magnetic field are

$$\begin{aligned} &U_2^2=U_{-2}^2=\tfrac{1}{2}, \quad U_1^2=U_{-1}^2=0, \quad U_0^2=1/\sqrt{6}, \\ &U_1^1=U_{-1}^1=U_0^1=0, \quad U_0^0=1/\sqrt{3}, \end{aligned} \tag{A6}$$

and when the detected light is polarized parallel to the direction of the magnetic field, they are

$$\begin{aligned} &U_2^2=U_1^2=U_{-1}^2=U_{-2}^2=0, \quad U_0^2=-2/\sqrt{6}, \\ &U_1^1=U_{-1}^1=U_0^1=0, \quad U_0^0=1/\sqrt{3}. \end{aligned} \tag{A7}$$

The $L=1$ component of the polarization tensor is always zero in this geometrical configuration. Substituting for the coefficient B_L from Tables V–VII and Eqs. (A5)–(A7) in Eq. (10), we find that the intensity of the unpolarized fluorescent light for the case in which the excited state branches exclusively to a single branch state is

$$R=\alpha\left(1-\beta\frac{1-4\omega_e\omega_b\tau_e\tau_b}{(1+4\omega_e^2\tau_e^2)(1+4\omega_b^2\tau_b^2)}\right)\frac{R_0\Gamma_{eb}\Gamma_{bf}}{8\pi\Gamma_e\Gamma_b}, \tag{A8}$$

where the coefficients α and β for various cases are listed in Table VIII. When the fluorescent light detected is along the direction perpendicular to both the exciting light and the magnetic field, the intensity is given by Eq. (A8) in which β is replaced with $-\beta$. The signal R in this case depends on the magnetic field H through the following relation:

$$R=\alpha\left[1+\beta\left(\frac{1-4(\mu_0/\hbar)^2(g_e\tau_e)(g_b\tau_b)H^2}{[1+(2g_e\tau_e\mu_0H/\hbar)^2][1+(2g_b\tau_b\mu_0H/\hbar)^2]}\right)\right]\times\frac{R_0\Gamma_{eb}\Gamma_{bf}}{8\pi\Gamma_e\Gamma_b}. \tag{A9}$$

TABLE VI. $J_i=2$, $J_e=2$, $J_b=1$, $J_f=0$.

L	$W(221L;12)$	$W(121L;12)$	$W(L110;11)$	$B_L/\Gamma_{eb}\Gamma_{bf}R_0$
2	$-\sqrt{7/300}$	$7/\sqrt{300}$	$\frac{1}{3}$	$-21/160\pi$
1	$1/\sqrt{180}$	$1\sqrt{20}$	$\frac{1}{3}$	$3/32\pi$
0	$1/\sqrt{15}$	$1/\sqrt{15}$	$\frac{1}{3}$	$3/8\pi$

TABLE VIII. Values of α and β appearing in Eq. (A8).

J_i	J_e	J_b	J_f	β	α
2	1	1	0	$\frac{9}{243}$	$\frac{243}{120}$
2	2	1	0	$\frac{21}{87}$	$\frac{87}{40}$
0	1	1	0	$\frac{1}{3}$	$\frac{9}{4}$

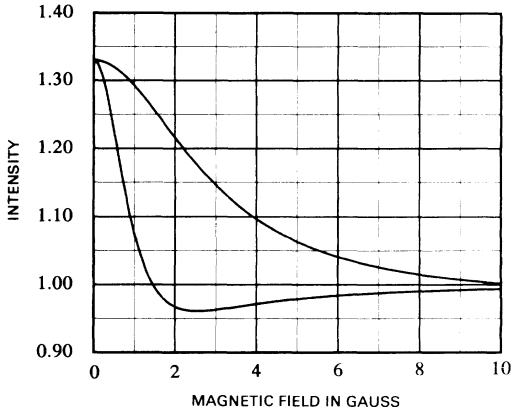

FIG. 9. Theoretical plots of R from Eq. (A9) for branching to a single state. The values used in the plots are (1) upper curve $g_e = 1$, $g_b = 1.034$, $\tau_e = 19.5$ nsec, $\tau_b = 1.5$ nsec; (2) lower curve $g_e = 1.984$, $g_b = 1.464$, $\tau_e = 26.45$ nsec, $\tau_b = 20$ nsec. $A = 1$ and $B = 0.33$ for both curves.

When the exciting light is polarized parallel to the magnetic field, the only nonzero components of E_M^L are E_0^2 and E_0^0 [see Eq. (A7)]. Therefore, in Eq. (10) only $M = 0$ terms contribute and R becomes field independent.

R is symmetric with respect to the interchange of $g_e\tau_e$ and $g_b\tau_b$. The shape of the signal computed from Eq. (A9) corresponding to some typical experimental situation (assuming branching to a single state) is shown in Fig. 9. The values of the atomic parameters used in the calculations are indicated on the figure. For the case in which $\tau_e \simeq \tau_b$ the cascade-fluorescence signal falls off rapidly as the magnetic field is increased until $H = H_M$ where the signal is minimum. As the magnetic field is further increased the signal increases slowly to the asymptotic value. When $\tau_b \ll \tau_e$, the signal monotonically falls off to the asymptotic value without reaching a minimum, and furthermore the half-width is much larger than in the other case. The magnetic field H_M where the cascade-fluorescence signal reaches a minimum is obtained from solving the equation $\partial R/\partial H$ and is found to be

$$H_M^2 = \frac{1}{4\Omega_e\Omega_b}\left(1 + \frac{\Omega_e + \Omega_b}{(\Omega_e\Omega_b)^{1/2}}\right), \qquad \text{(A10)}$$

where

$$\Omega_e = (\mu_0/\hbar)g_e\tau_e\,, \quad \Omega_b = (\mu_0/\hbar)g_b\tau_b\,. \qquad \text{(A11)}$$

In (A9) β essentially determines the ratio of the magnetic-field-dependent to the field-independent part of the signal, and in certain cases β is quite small. This ratio can be increased if one detects polarized fluorescent light instead of unpolarized light. However, in our experiment, the detected cascade-fluorescent radiation lies in the XUV range (744 and 736 Å) and no suitable polarizers are available for this wavelength.

In the preceding discussion we limited ourselves to the case in which the cascade-fluorescent signal from a single branch state was detected. Even if the excited state decays to more than one branch state, the case discussed above is experimentally valid provided one detects the photons from a specific branch state b to the final state. The present experiment reported in this paper does not satisfy this requirement. The optically excited state decays to two branch states and the initial state. The cascade fluorescent signal that is detected consists of XUV photons emitted from the spontaneous decay of the two branch states to a single final state. The photon detector counting the cascade-fluorescent photons has very nearly the same sensitivity for these two wavelengths (744 and 736 Å). Since direct dipole transition between the initial and final state is forbidden, the partial decay of the excited state back to the initial state has no effect on the detected signal. The contribution to the cascade-fluorescent signal due to the two channels of decay of the excited state to the branch states is the weighted sum of the individual contributions, the ratio of the weighting factors being proportional to the branching ratio. In our experiment the total angular momentum of each of the two branch states is the same (viz., $J = 1$) and hence the coefficients α and β in (A10) is the same for both channels of decay. However, $g\tau$ for the two branch states are quite different. The cascade-fluorescent signal for such a case is just the sum of two terms of the form given in Eq. (A8) or (A9).

APPENDIX B

The effect of alignment of the initial state on the cascade Hanle signal is discussed here. Our initial states are the metastable states $1s_3(^3P_0)$ and $1s_5(^3P_2)$ of neon produced by electron bombardment of the ground-state ($^1S_0$) atoms. It is well known that electron excitation can produce alignment in the metastable states. For electron energies near the threshold, $\Delta M_J = 0$. In the case of neon, the $M_J = 0$ level of the metastable state will be produced more preferentially if one neglects the electron exchange effect. Electron-exchange results in $\Delta M_J = \pm 1$. Electron excitation produces only alignment; not polarization.

As discussed earlier the effect of alignment of the initial state on the cascade Hanle effect can be studied by introducing the exciting light polarization tensor $\mathcal{E}_M^L$ instead of E_M^L. $\mathcal{E}_M^L$ is defined in Eq. (16). Separating the $\Lambda = 0$ term, we can write

$$\mathcal{E}_M^L = E_M^L + \sum_{\Lambda=1}^{2J_i} \sum_{L'=0}^{2} (-1)^{L'-L}(2J_i+1)\frac{[(2\Lambda+1)(2L'+1)]^{1/2}}{W(J_i J_e 1L; 1J_e)} \begin{bmatrix} 1 & J_e & J_i \\ 1 & J_e & J_i \\ L' & L & \Lambda \end{bmatrix} [E^{L'}(\rho^i)^\Lambda]_{LM} \tag{B1}$$

and

$$[E^{L'}(\rho^i)^\Lambda]_{LM} = \sum_{M'} E_{M'}^{L'}(\rho^i)^\Lambda_{M-M'} C(L'\Lambda L; M'M-M')(-1)^{M'-M-L}. \tag{B2}$$

In the case of alignment and no coherence in the initial state, it can be quite easily shown that only $(\rho^i)^\Lambda_{\Lambda=0}$ terms contribute. Furthermore, $(\rho^i)^0_0, (\rho^i)^2_0, (\rho^i)^4_0, \ldots, (\rho^i)^{2J_i}_0$ are the only nonzero components for J_i = integer and $(\rho^i)^0_0, (\rho^i)^2_0, \ldots, (\rho^i)^{2J_i-1}_0$ are only nonzero components for J_i = half-integer. For neon only integer values of J_i need be considered. Making use of the properties of the 3-j amd 9-j symbols, we obtain the following expressions for the components of the effective light polarization tensor:

$$\mathcal{E}_0^0 = E_0^0 + \frac{5(2J_i+1)}{W(J_i J_e 10; 1J_e)} \begin{bmatrix} 1 & J_e & J_i \\ 1 & J_e & J_i \\ 2 & 0 & 2 \end{bmatrix} C(220; 00)(\rho^i)^2_0 E_0^2, \tag{B3}$$

i.e., $\mathcal{E}_0^0$ is a linear combination of E_0^0 and E_0^2. Similarly,

$$\mathcal{E}_M^1 = E_M^1 \left\{ 1 + \frac{\sqrt{15}(2J_i+1)}{W(J_i J_e 11; 1J_e)} \begin{bmatrix} 1 & J_e & J_i \\ 1 & J_e & J_i \\ 1 & 1 & 2 \end{bmatrix} C(121; M0)(\rho^i)^2_0 \right\} \tag{B4}$$

for $M = 0, \pm 1$. $\mathcal{E}_M^1$ is zero whenever E_M^1 is zero. Since $C(121; M0)$ is independent of the sign of M, the factor with the curly brackets in Eq. (B4) is the same for $M = +1$ and -1.

Finally,

$$\mathcal{E}_M^2 = E_M^2 \left(1 + \frac{(2J_i+1)}{W(J_i J_e 12; 1J_e)} \left\{ C(242; M0)(\rho^i)^4_0 3\sqrt{5} \begin{bmatrix} 1 & J_e & J_i \\ 1 & J_e & J_i \\ 2 & 2 & 4 \end{bmatrix} + C(222; M0)(\rho^i)^2_0 5 \begin{bmatrix} 1 & J_e & J_i \\ 1 & J_e & J_i \\ 2 & 2 & 2 \end{bmatrix} \right\} \right)$$
$$+ \frac{(2J_i+1)\sqrt{5}}{W(J_i J_e 12; 1J_e)} \begin{bmatrix} 1 & J_e & J_i \\ 1 & J_e & J_i \\ 0 & 2 & 2 \end{bmatrix} E_0^0 (\rho^i)^2_0 C(022; 00). \tag{B5}$$

We observe that $\mathcal{E}_M^2$ for $M \neq 0$ is directly proportional to E_M^2 and the constant of proportionality is independent of the sign of M. $\mathcal{E}_0^2$ is a linear combination of E_0^2 and E_0^0. The alignment of the initial state influences the cascade Hanle effect only through two independent parameters $(\rho^i)^2_0$, and $(\rho^i)^4_0$. The expression for the cascade-fluorescent signal is

$$R = \sum_{LM} (-1)^M \frac{B_L \mathcal{E}_M^L U_{-M}^L}{(\Gamma_e + iM\omega_e)(\Gamma_b + iM\omega_b)}. \tag{B6}$$

The magnetic-field-dependent terms are for $M \neq 0$. For our experimental configuration [Eq. (A5)] $E_M^1 = 0$ for all M and $E_M^2 = 0$ for $M = \pm 1$. Expanding (B6) and substituting for $\mathcal{E}_M^L$ in terms of E_M^L, it can be shown that R retains the same magnetic field dependence as (A8). The only difference is that the constants α and β are different. In other words, the observed cascade Hanle signal retains the same shape independent of alignment of the initial state, although the amplitude of the signal depends on the degree of alignment.

*This paper is based on a thesis submitted to Columbia University by N. D. Bhaskar.

†Present address: Department of Physics, New York University, New York, N.Y. 10003.

[1]N. Schütz, Ann. Phys. (Leipzig) 18, 705 (1933).
[2]A. V. Phelps, Phys. Rev. 100, 1230 (1955).
[3]F. A. Korolev, V. I. Odintsov, and E. V. Fursova, Opt. Spektrosk. 16, 555 (1964) [Opt. Spectrosc. 16, 304

(1964)].
[4]H. Kuhn, E. Lewis, Proc. R. Soc. Lond. A 299, 423 (1967); E. Lewis, Proc. Phys. Soc. Lond. 92, 817 (1967).
[5]G. M. Lawrence and H. S. Liszt, Phys. Rev. 178, 122 (1969).
[6]J. De Jongh and J. Van Eck, Physica (Utr.) 51, 104 (1971).
[7]S. Kazantsev and M. Chaika, Opt. Spektrosk. 31, 510 (1971) [Opt. Spectrosc. 31, 273 (1971)].
[8]J. Kernahan, A. Denis, and R. Drouin, Phys. Scripta 4, 49 (1971).
[9]D. Irwin, A. Livingston, and J. Kernahan, Can. J. Phys. 51, 1948 (1973).
[10]E. Knystautas and R. Drouin, Astron. Astrophys. 37, 145 (1974).
[11]A. Gold and R. Knox, Phys. Rev. 113, 834 (1959).
[12]M. Aymar, S. Feneuille, and M. Klapisch, Nucl. Instrum. Methods 90, 137 (1970).
[13]P. Gruzdev and A. Loginov, Opt. Spektrosk. 33, 1191 (1972) [Opt. Spectrosc. 33, 650 (1972)].
[14]A. Corney, in *Advance in Electronics and Electron Physics* (Academic, New York, 1970), Vol. 29, pp. 115–231.
[15]C. G. Carrington and A. Corney, J. Phys. B 4, 849 (1971).
[16]M. Ducloy and M. Dumont, J. Phys. (Paris) 31, 419 (1970).
[17]C. G. Carrington, J. Phys. B 5, 1572 (1972).
[18]R. Gupta, S. Chang, and W. Happer, Phys. Rev. A 6, 529 (1972).
[19]W. Happer (private communication); Rev. Mod. Phys. 44, 169 (1972).
[20]W. Happer and B. Mathur, Phys. Rev. 163, 12 (1967).
[21]M. E. Rose, *Elementary Theory of Angular Momentum* (Wiley, New York, 1957).
[22]J. Burger and A. Lurio, Phys. Rev. A 3, 64 (1971).
[23]J. Bridges and W. Wiese, Phys. Rev. A 2, 285 (1970); S. Inatsugu and J. Holmes, *ibid.* 11, 26 (1975).
[24]Philip R. Bevington, *Data Reduction and Error Analysis for the Physical Sciences* (McGraw-Hill, New York, 1969), Chap. 11.
[25]R. Arndt and M. H. MacGregor, *Methods in Computational Physics* (Academic, New York, 1966), Vol. 6, p. 253–296.
[26]F. Dunning, T. Cook, W. P. West, and R. Stebbings, Rev. Sci. Instrum. 46, 1072 (1975).